CHAPTER 6
Radar Remote Sensing of Mangrove Forests

Marc Simard, Senior Scientist,Radar Science and Engineering Section, Jet Propulsion Laboratory, California Institute of Technology

ABSTRACT

Mangrove forests are highly productive ecosystems providing critical ecosystem services. It is estimated that about a third of mangrove forests have been lost during the last century and are still being decimated at a rate of about 0.4% per year. Mangrove forests are thin strips of forests living along tropical coasts. These environments are generally cloudy; optical remote sensing instruments provide limited temporal coverage to ensure consistent monitoring of mangrove health and status. Radar remote sensing enables all-weather monitoring of mangrove forest gain and loss in extent. In addition, it can observe several parameters related to vertical canopy structure and biomass. The first part of this chapter introduces mangrove forests and the state-of-the-art radar remote sensing techniques to measure and monitor mangrove forest structure. The second part of this chapter presents a step-by-step tutorial on the use of radar remote sensing to make these measurements. After this chapter, the reader will be able to perform analysis of radar images of mangrove forests and more.

6.1 Introduction to Mangrove Forests

Mangrove forests are some of the most productive ecosystems in the world. They thrive within the intertidal zone along the coasts of tropical and subtropical regions (**Fig. 6.1**). Mangrove trees can sustain salt water and soils with low oxygen availability through root adaptations. They were recently included in the Intergovernmental Panel on Climate Change (IPCC) climate mitigation strategy through the Wetland supplements. While mangrove forests cover a small land area (<1%), they may be responsible for 10% of global carbon export to oceans (Jennerjahn and V. Ittekkot 2002). Most importantly, mangrove forests provide numerous ecosystem services that sustain the livelihood of millions of people (Barbier et al. 2011). Some of these services, in addition to carbon sequestration, include protection of coastline and infrastructure against severe storms and tsunamis, nursery of fish and crustaceans, and the production of lumber and charcoal.

Mangrove forests occupy terrestrial and marine environments, enabling them to support a very broad range of biodiversity. This biodiversity ranges from organisms within the soil to high numbers of fish spe-
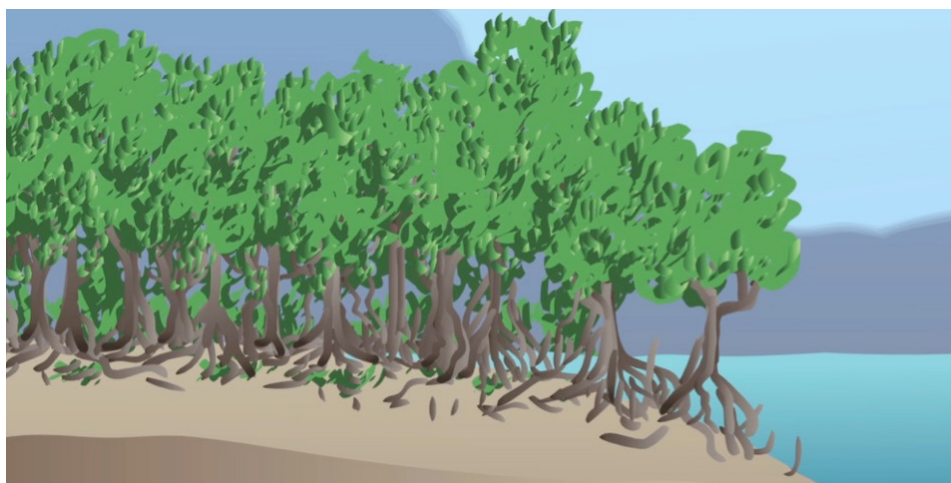

Figure 6.1 Mangrove forests occupy the intertidal zone between approximately mean water to high tide. Assuming a flat ground at sea level is generally a good approximation (Image credit: Maria Raykova).

cies to terrestrial species including reptiles, mammals, birds, and insects. Mangroves provide both direct and indirect services to local populations that inhabit the coastal zone. Several products can be directly sourced from the mangrove that have both a subsistence use and economic value. Primary benefits include sediment trapping; the production of nutrients and organic matter through detritus; a sink for carbon, nitrogen, and phosphorus; maintaining water quality; provision of food and habitat for biodiversity; and

providing shoreline protection from storms and rising sea levels (e.g., Quoc Tuan et al. 2012). Mangroves have been demonstrated to provide greater long-term economic benefits to local households through their preservation, compared to the short-term economic gains through their destruction for products (McNally et al. 2011). An important reason for conversion of mangroves is shrimp farming, driven by economic incentives as mangrove is often regarded as wasteland (Primavera 2000). The level of services often depends

on forest structure and, therefore, structural parameters such as height and basal area. For example, tall forests provide more protection against strong winds, store more carbon, and can provide more lumber and coal. Mangrove structure should therefore be considered when mangrove economical value is assessed.

Mangroves can exceed 60m in height and are subsequently able to attain high values of above ground biomass (AGB) around the 800 Mg ha^{-1} mark (Simard et al. 2019). These values rival observations in other types of tropical forests. Their elevated Net Primary Productivity (NPP) contribute large amounts of organic carbon inputs into the underlying soil. Thanks to slow anaerobic decomposition, mangrove forests store disproportionate amounts of carbon in their soils. Mangrove ecosystems are estimated to be amongst the most carbon rich ecosystems within the tropics, storing an average of 1,023 Mg C ha^{-1} in shallow soil depth ranging from 0.5–3 m (Donato et al. 2011). At current mangrove loss rates, between 0.02–0.12 Pg per year is released to the atmosphere, that is 10% of total carbon emissions from deforestation despite accounting for less than 1% of tropical forest area (Donato et al. 2011). Hamilton et al. (2016) estimate current global loss between 0.16 and 0.39%. Thus, they play a significant role in the carbon cycle and consequently are becoming economically viable to protect (Murray 2012, Jerath 2012, Pendleton et al. 2012). Initiatives, such as the Reducing Emissions from Deforestation and forest Degradation plus (REDD+) are carbon accrediting programs, whereby the carbon stored within natural ecosystems is valued by its ability to offset anthropogenically produced CO_2. This payment for ecosystem services (PES) initiative extends beyond the worth of carbon to other services such as their resilience to hazards and role in maintaining fish biodiversity and water quality (Locatelli et al. 2014). The inclusion of mangroves in such initiatives can make them profitable environments, enhancing the socioeconomic benefits of mangrove forests beyond subsistence use to an asset for all global citizens.

There are several environmental drivers of mangrove structure, mainly, precipitation and temperature (Simard et al. 2019) and the availability of nutrients and salinity (Castañeda-Moya et al. 2013). Local geophysical characteristics such as microtopography

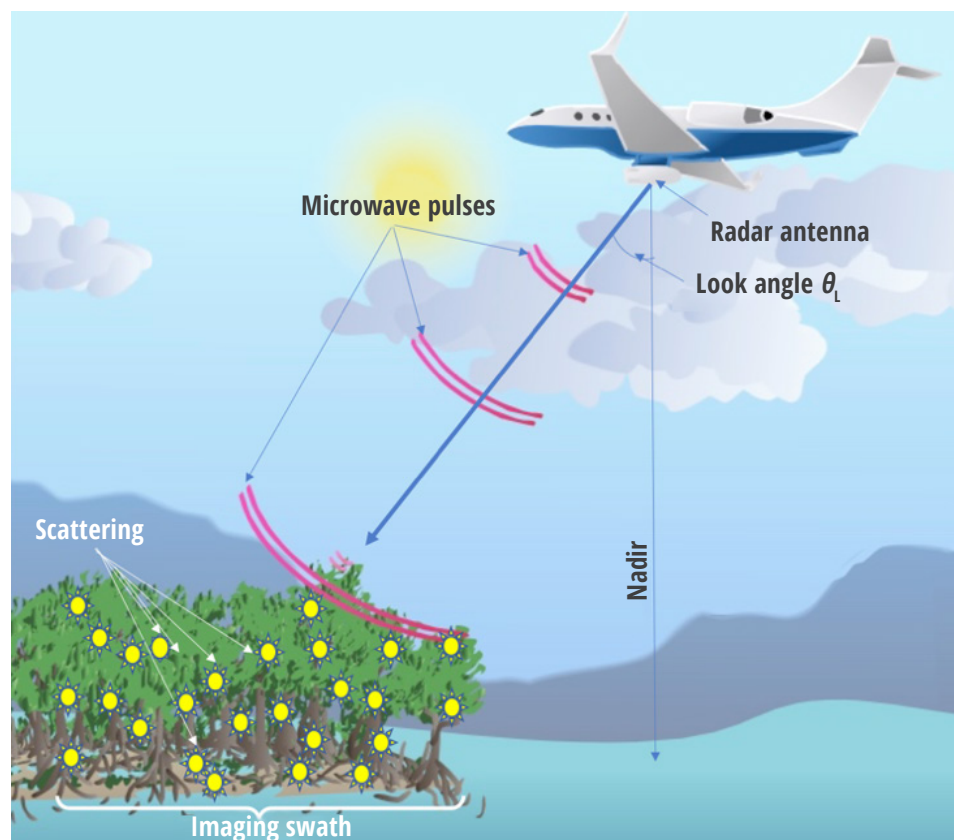**Figure 6.2** *Global distribution of mangrove forests (From Giri et al. 2010).*

Figure 6.3 *Radar imaging, whether airborne or spaceborne, is performed by transmitting a microwave pulse 'sideways' that scatters with land features such as forest branches, trunks roots, and ground. The imaging swath illuminated by one pulse determines the image size in the cross-track (or range) direction. (Background image credit: Maria Raykova) Additional information on how SAR images the world can be found in* **Chapter 2**.

and freshwater availability strongly control salinity and hydroperiod, and thus mangrove NPP (Castañeda-Moya et al. 2013). However, microtopography is very difficult to estimate at the landscape scale and cannot be observed directly from spaceborne remote sensing. On the other hand, remote sensing can measure the ecosystem response to these geophysical variables, reflected in observed canopy height, spe-

cies distribution, and spatial patterns.

Despite their importance for carbon storage, biodiversity, and supporting indigenous local communities, mangrove forests are threatened across their entire range (Thomas et al. 2017). Mangrove areal extent for the nominal year 2000 was 13.7 million ha, far below the previous 1980 estimate of 18.8 million ha (FAO 2007) (**Fig. 6.3**). The rate of mangrove

loss throughout the 1990s was estimated as 1% yr⁻¹; a rate twice that of terrestrial rainforest over the same period (Mayaux et al. 2005). Recently, Hamilton and Casey (2016) found the yearly loss of mangrove extent between 2000–2012 varying between 0.16 and 0.39%. Comparatively, 30% of total tropical terrestrial forest has been lost as a consequence of anthropogenic activity since monitoring began, while it is estimated that one third of total mangrove forest has been lost over the last half-century alone (Alongi 2002). Unfortunately, the loss of mangroves across the globe is deemed critical enough that 11 of the true 70 mangrove species have met the criteria of the Red List categories of threat (Polidoro et al. 2010).

The largest driver of this loss has been the conversion of mangrove forests to aquaculture. In an assessment of mangrove forest extent and loss at a variety of locations in the Americas, Africa, Asia, and Australia, the greatest cause of mangrove loss was evaluated to be due to mariculture practices. 52% of 36 x 10³ km² of the estimated loss from within countries containing 66% of the total area of mangrove forests was caused by shrimp cultivation (Valiela et al. 2001). Aquaculture is the fastest growing animal-food sector in the world. In 2011, fish from aquaculture practices accounted for nearly half of the total fish consumed worldwide (45.6%). Aquaculture has a plethora of direct and indirect detrimental impacts upon a mangrove forest. These include the immediate loss of mangroves for pond construction alongside the alteration of natural tidal flows, release of toxic wastes, reduced water quality and alterations to sedimentation rates, and turbidity. Additional pressures upon mangroves include the development of the coastal zone that causes the direct replacement of mangrove and a suite of associated environmental problems, such as pollutants in runoff. Furthermore, the coastal zones of the world are becoming increasingly populated, and the current trends of increasing global population will put further demands upon mangrove forests (FAO 2013, FAO 2012).

As we move increasingly through an era of unprecedented climate change, Earth's climate will undergo changes that are currently not known with certainty. Sea level rise is expected to continue and accelerate over the coming century, with an increase in mean sea level by as much as 1 m by 2100 (CITATION). Although sea level rise will not be uniform throughout the oceans, 70% of the world's coastlines are estimated to experience sea level rise within 20% of the global mean (IPCC AR5). Mangroves are known to accrete sediment (Cheong et al. 2013) by trapping sediment suspended when inundated or through the build-up of peat through the decomposition of organic matter (Krauss et al. 2014). The survival of mangrove forests in the face of sea level rise is therefore dependent on whether sediment is accreted at the same rate as sea level rise (McKee et al. 2002, Hashimoto et al. 2006). Should sea levels rise above the rate of the terrestrial surface, mangroves will either face periods of longer inundation or will migrate landwards into new areas. It is not currently known how climate change will affect the atmosphere and subsequent terrestrial processes, making the extrapolation of all the effects of climate change on mangrove forests difficult. Precipitation is expected to be spatially variable, with increasing climate change and growing contrast between wet and dry regions and between seasons (IPCC AR5). The impact of increasing precipitation is expected to have a positive effect on growth rates, biodiversity, and mangrove extent as they migrate into previously drier environments (Eslami Andargoli et al. 2009). An increase in precipitation will also decrease the salinity of the environment and is expected to lead to an increase in species richness and diversity (Asbridge et al. 2015). In contrast, a decrease in precipitation will increase the salinity of mangrove environments and cause an overall decrease in mangrove area as freshwater influxes become too saline to support growth (Duke et al. 1998, Gilman et al. 2008). Decreases in precipitation are also likely to cause a reduction in photosynthesis as a consequence of increased aridity (Arreola Lizarraga et al. 2004). Atmospheric temperatures will increase by as much as 2°C by the end of 2100 and are forecast to increase further thereafter (IPCC AR5). Changes in atmospheric temperature can be expected to cause an expansion of mangroves into higher latitudes and change the species composition and distribution of mangrove forests (Soares et al. 2012, Wilson and Saintilan 2012, Saintilan et al. 2014). The effects of climate change on mangrove forests are difficult to accurately predict due to the complexity of the natural system and complex feedbacks.

Traditionally, large-scale mangrove mapping was limited to sketch maps, fieldwork maps, and the digitizing of digital datasets (Spalding et al. 1997). Yet over the past years, the number of studies on mangrove extent, change, ecosystem structure, ecosystem services, and vulnerability derived from remote sensing have proliferated (Kuenzer et al. 2011). The first global map exclusive to mangrove forests that used remotely sensed data alone was that of Giri et al. (2011). This work processed over 1,000 Landsat scenes gathered over the period 1997–2000, and estimated the total mangrove extent to be 13,776,000 ha despite the methodology suffering from a number of limitations. Since then, changes have occurred and been detected at global scales (Lucas et al. 2014, Thomas et al. 2017, and in maps by Hansen et al 2013). Products that incorporated annual estimates of mangrove extent followed, such as the CGMFC-21 (Hamilton and Casey 2016, Hutchison et al. 2014), with a much higher temporal resolution. In addition, there have been many regional, country-scale, and project-scale assessments of mangrove extent, change, and three-dimensional structure using both optical and passive remotely-sensed data (Fatoyinbo and Simard 2008, Fatoyinbo et al. 2013, Spalding et al. 2010, Simard et al. 2019).

There is a plethora of remotely sensed data available for mapping mangrove extent and change, which has the potential for long-term monitoring of land-use change and the identification of proximate drivers of change. These include the Landsat time-series, now enhanced by the European Space Agency (ESA) Sentinel-2 platforms, that, when combined, offer an unprecedented quantity of data. Similarly, radar data is available from ESA via the Sentinel-1 satellites and annual mosaics from the Japan Aerospace Exploration Agency's (JAXA's) Advanced Land Observing Satellite 2 (ALOS-2) platform. Historic radar imagery to aid in time-series mapping is freely available via ALOS and Japanese Earth Resources Satellite 1 (JERS-1) mosaics (See **Table 2.5, Chapter 2**). These will soon be followed by the joint NASA-ISRO Synthetic Aperture Radar (NISAR) mission planned for launch in December 2021. It is therefore timely to develop
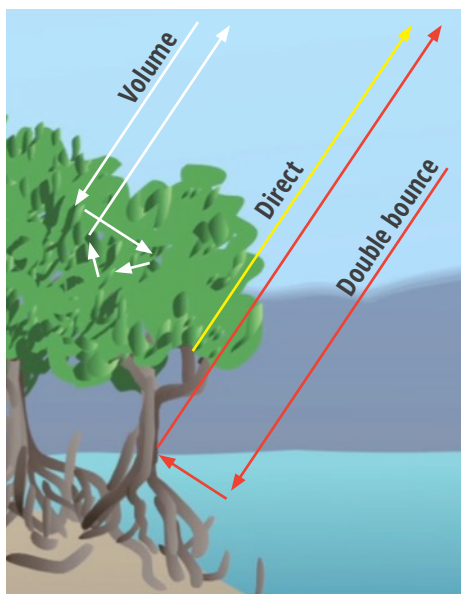
Figure 6.4 *Radar scattering mechanisms. In mangrove forests with aerial roots (Rhizophora), the microwave signal is attenuated, decreasing backscatter at high biomass.*
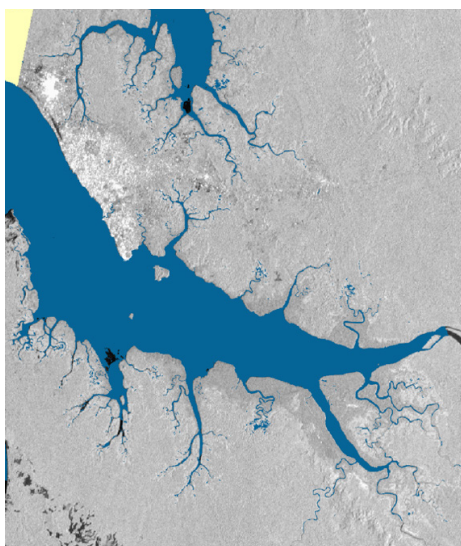

Figure 6.5 *Radar backscatter at L-HH, acquired by ALOS-2 over the Gabon Estuary, Gabon. Bright areas to the North West result from strong double-bounce effect in urban structures of the city of Libreville. Large medium backscatter (mid-gray tones) are due to volume scattering in forests. Water was easily masked based on darker backscatter (in particular at LHV). Interestingly, due to strong attenuation from roots, tall mangrove forests with red mangrove trees reaching several tens of meters exhibit lower backscatter along the South Eastern portion of the Estuary.*

new remote sensing algorithms that combine optical and radar data for long-term monitoring of mangroves forests in Southeast Asia.

6.2 Radar Remote Sensing

A radar instrument generates its own electromagnetic signal by transmitting a microwave pulse that enables observation of Earth's surface (or other planets and moons) day and night. In order to generate an image, the pulse is focused in a direction away from nadir (**Fig. 6.3**). When the pulse is transmitted at nadir, the instrument is called a radar altimeter. The microwave pulse typically illuminates ground areas of tens of kilometers, and only the portion of energy reflected toward the radar is measured. The angular reflection pattern depends on the target properties such as roughness (differs greatly between plants, water surface, urban structures) and geometry. The geometry is determined by the look angle and the terrain slope. The former is the angle subtended by the line of sight between the radar and a target on the ground. Thus, it varies greatly across an image. The look angle and terrain slope can be combined into the incidence or projection angle. These angles are often used to perform terrain radiometric corrections (sometimes called 'terrain flattening'), which is intended to remove image artifact due to geometry. In mangroves, topographic effects are generally neglected due to their unique setting of very flat areas.

6.2.1 MICROWAVE BANDS

Radars are active instruments with a definite advantage over optical sensors: they can see through clouds, day and night. This is a particularly prized attribute along the tropical coastlines, and its free public availability is continuously rising. They transmit a microwave pulse and measure the portion of the energy that is reflected back. The measured return is called "backscatter" and is generally presented in decibels ($10\log_{10}$(Intensity)). Some Radar instruments come in several "colors" (i.e., wavelength bands): Ka and Ku-bands, X-, C-, S-, L-, and P-bands. Those are denominations introduced during the development of radar during World War II, and they simply refer to a range of frequencies as defined by

the Institute of Electrical and Electronics Engineers (IEEE). See **Table 2.3 in Chapter 2** to see common applications of SAR bands.

6.2.2 SCATTERING MECHANISMS IN MANGROVES

There are three types of scattering mechanisms: (1) direct (or single bounce), (2) double-bounce, and (3) volume scattering (see **Fig. 6.4**). In mangrove forests, the "double-bounce" term that strongly impacts the HH channel (see **Chapter 2, Table 2.3**, relative scattering strength by polarization, and the subsequent section) may be reduced by the presence of aerial roots as microwaves are scattered and attenuated (**Fig. 6.5**). The dominant scattering mechanism in mangrove forest strongly depends on canopy structure. Trends in volume and double-bounces' signatures vary much more than in other types of forests. In particular, in mangroves the volume scattering decreases and double-bounce scattering increases in closed and open canopies, respectively (see following section on polarimetry). Inundation at the time of data acquisition impacts radar signals in open mangrove forests.

6.2.3 POLARIMETRY

The radar measurement can also be characterized through polarimetry. Generally, radar instruments are enabled for several orthogonal polarimetric modes, transmitting horizontal (H) or vertical (V) polarization, and receiving either H or V. For example, an L-band radar transmitting a horizontally polarized microwave and receiving its vertical polarization would be identified as L-HV. A single instrument can collect data in several polarimetric mode by alternating pulses. A quad-pol L-band radar collects four channels: L-HH, L-HV, L-VH, and L-VV (e.g., **Fig. 6.6**). Upcoming instruments like the Radarsat constellation suite of instruments will provide circular polarization, indicating that polarization state changes in time. Each polarimetric configuration can be considered as an image band in the radar dataset, each sensing various characteristics of the forest canopy through the variety of scattering mechanisms. While the HV measurement is dominated by the volume scattering reflections, the HH and VV contain a significant ground contribution.

In particular, the HH polarization is strongly impacted by the occurrence of double-bounce scattering, which is greatly enhanced by the presence of water. As such, it is important to note the contribution from double-bounce scattering in mangrove forests can be greatly reduced by the presence of aerial roots. *More about polarimetry in* **Chapters 2 and 3**.

Early work on polarimetry at C-, L-, and P-band (e.g., Mougin et al. 1999, Proisy et al. 2002) has shown that the relative impact of the scattering mechanisms changes significantly with radar wavelength, with ground and double-bounce contributions increasing wavelength. Polarimetry has been demonstrated as a powerful method to classify wetland types, including mangroves at X-band (e.g., Hong et al. 2015), and mangrove species and structure at L-band (e.g., Brown et al. 2016) and C-band (e.g., Kovacs et al. 2013, Cougo et al. 2015). There are several models to obtain the relative contribution of the three scattering mechanisms. A popular one is the Freeman-Durden decomposition (available in SNAP and PolSARpro software) used in Proisy et al. (2002). **Figure 6.7** shows the decomposition of a fully polarimetric radar image acquired by the UAVSAR's L-band airborne radar instrument. In the top left image of **Figure 6.7**, the brown areas represent low double interaction found in tall Rizhophora mangrove forests, and shades of blue are found in more open and shorter shrub mangroves. Green tones, representing dominance of volume scattering, are found in inland forests. Otherwise red tones, representing dominance of single bounce, occur over open land surfaces. The individual contribution of each scattering mechanism is shown in grey-scale images in **Figure 6.7**. Contrary to inland forests, the volume component is reduced in tall mangrove forests and increased with shorter ones. While the volume component (or even at HV polarization) may become similar to that of inland forests, the apparent texture of mangrove forests is much smoother, in part due to inland topography and to overall homogeneity of mangrove canopy structure. Thus, polarimetric signature can be used to identify mangrove forests from other landcover types, particularly at longer wavelengths (e.g., L-band), and also differentiate mangrove structural attributes and species.
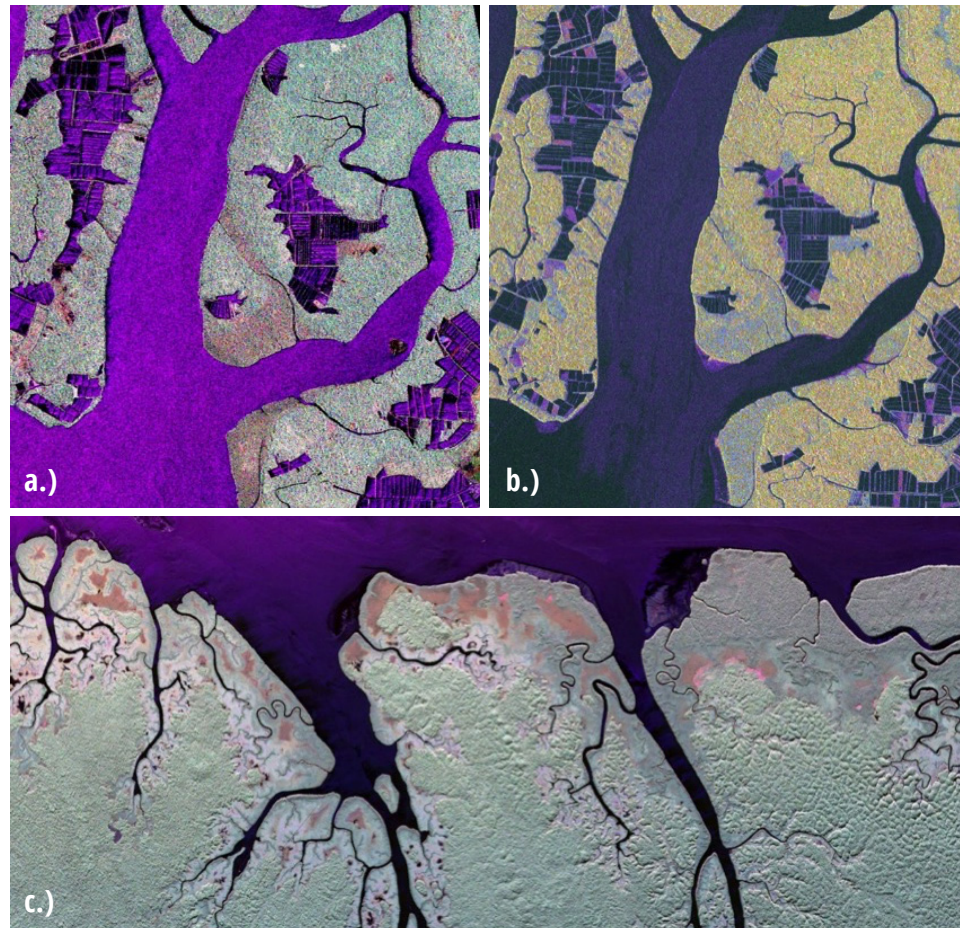

Figure 6.6 *Color composite images of mangrove forests of the Guayas Estuary in Ecuador from: a) ALOS-PALSAR-1 HH, HV, and VV in RGB, respectively; b) Sentinel-1 VV, VH, and VV in RGB, respectively. Volume scattering dominates at all polarization and at both L- and C-band. Lower backscatter is observed for the younger, low-density forest (<100t/ha) found along the coast at the bottom of the images. Figure 6c) shows a color composite (HH, HV, VV) of a 6-m resolution L-band airborne UAVSAR image acquired in the Gabon Estuary showing the distinct signature of mangrove forest whether tall (east) or short shrub forest (west). Green indicates the dominance of HV in inland forest is more significant than in mangrove forest where all polarization configurations (HH, HV, and VV) behave similarly, resulting in the observed grey level intensities.*
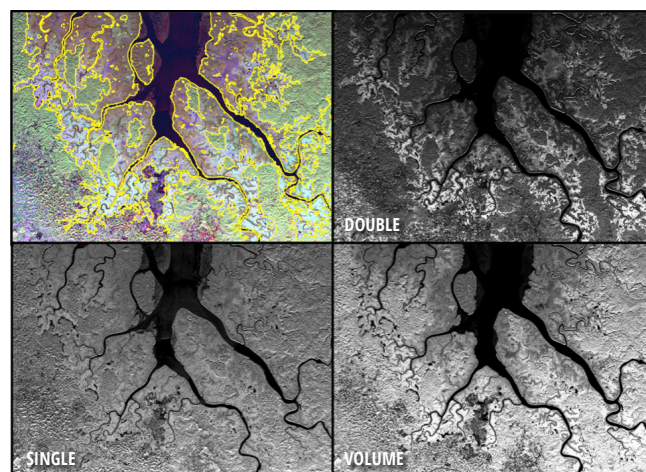

Figure 6.7 *Polarimetric representation of mangrove forests in Akanda, Gabon. Top left image shows an RGB color composite image of single, volume, and double-scattering components based on the Freeman-Durden decomposition. The yellow polygons show the mangrove extent.*

6.2.4 INTERFEROMETRY

Radars can operate in interferometric mode, which means the measurement is obtained from several individual observations of the same target, viewed from different radar antenna positions. These individual observations can be collected simultaneously with pairs of radar antennas, or with a single antenna operating in repeat-pass mode. When observations are from a slightly different point of view, as in the pairs of radar antennas formation, the elevation can be estimated through geometry. The latter technique involves repeating an observation using the same instruments and combining measurements through interferometry (complex multiplication) to obtain coherence (a measure of the similarity of two images) and phase (relative location of scattering phase center between the two images). In addition, a pair of repeat-pass observations obtained from the same location (same instrument from same location but different time) enables measurements of changes in elevation or displacement of targets such as glacial flows, landslides, ground subsidence, etc. In the case of forest, zero-baseline repeat-pass interferometry is strongly impacted by 'temporal decorrelation,' which is a result of the motion of branches, changes in moisture, or growth. The zero-baseline interferometric measurement has been used to classify forest-age and structure of other types of forests (Simard et al. 2012, Pinto et al. 2012) as it strongly depends on forest height (Lavalle et al. 2012). Temporal decorrelation can impact repeat-pass non-zero baseline observation and must be compensated to obtain canopy height (Denbina et al. 2018).

Single-pass, non-zero baseline radar interferometry has been used to map mangrove canopy height (Simard et al. 2006, Simard et al. 2008, Fatoyinbo et al. 2013, Lagomasino et al. 2015, Lee et al. 2015, Simard et al. 2019). These maps express mangrove forest height using single-pass interferometric data obtained by the Shuttle Radar Topography Mission (SRTM) and TanDEM-X data (e.g., **Fig. 6.7**). The mangrove canopy height can then be translated into above ground biomass through in situ allometry relating biomass to canopy height (see section on mapping mangrove forest structure). On the other hand, repeat-pass interferometry can be used to identify structural attribute such as canopy stature and closure (e.g., **Fig. 6.9**).

RADAR BAND	SHRUB MANGROVES	TALL MANGROVES
P-HH	Around -17dB	Around -8dB (may increase with AGB)
P-HV and P-VH	Around -22dB	Around -14dB (may increase with AGB)
P-VV	Around -10dB	Around -7dB (may increase with AGB)
L-HH	-25dB to -15dB	Reduces from -5dB to -18dB with AGB
L-HV and L-VH	-25 to -20dB	Reduces from -15 dB to -22dB with AGB
L-VV	-20dB to -12 dB	Reduces from -8 to -16dB with AGB
C-HH	About -12dB	Varies about -7dB (no relationship to AGB)
C-HV	-20 to -15dB	varies about -14dB (no relationship to AGB)
C-VV	About -12dB	Varies about -6dB (no relationship to AGB)

Table 6.1 *General trends in radar backscatter for mangroves (Lucas et al. 2007, Proisy et al. 2002, Mougin et al. 1999). The trends are not constant and may exhibit increase for low biomass stands (shrubs) up to the standing forest where backscatter may decrease. Thus, the relationship between backscatter and biomass or height are not reliable biomass estimators.*

BAND	MANGROVE FOREST PENETRATION DEPTH	TYPE OF SCATTERING CAUSED BY MANGROVE FORESTS
K	Unknown; most likely a few tens of centimeters.	Single direct bounce and volume from top of canopy.
X	Interferometric measurement indicate penetration reaches, in the mean sense, Lorey's height (~1/3 of top forest height).	Single direct bounce and volume from top of canopy, with a small surface and double bounce component. The latter increase dramatically in open forests and at low biomass.
C	Comparison of SRTM C- and X-band show it is similar to C-band. Down to the equivalent of Lorey's height (~1/3 of top forest height)	Single direct bounce and volume from upper canopy, with a small surface and double bounce component. The latter increase dramatically in open forests and at low biomass.
L	Microwave penetration into canopy is as large as half the canopy height.	Single direct bounce dominates in tall forests, with volume dominating with shorter shrub mangroves. The contribution of double bounce increases significantly at low biomass and in open forests. In large red mangrove forest, with large aerial roots, microwaves will get absorbed and volume dominates again, although diminished.
P	Similar to L-band, where microwave penetration into canopy is as large as half the canopy height.	Single direct bounce dominates in tall forests, but the contribution of double bounces increases significantly at low biomass. In large red mangrove forest, with large aerial roots, microwaves will get absorbed and volume dominates again at biomass slightly larger than at L-band.

Table 6.2 *Microwave penetration depth and dominant scattering mechanisms in mangrove forests. Note this is in the mean sense as microwaves interacts with the entire canopy, all the way to the ground.*

6.2.5 RADAR DATA FORMAT

The availability of freely available radar data has increased significantly in the last decade (refer to **Table 2.5, Chapter 2**). Some datasets are calibrated and georeferenced science-ready products, and others are distributed at various levels of processing. There are multiple approaches to prepare the radar data, which depends on the original format of the data that has been downloaded. Generally, data is distributed with processing levels 1.0, 1.1, 1.5, or 2.0. The 1.0 and 1.1 format refer to backscatter in the radar geometry. That is, the images are not yet projected to geographic coordinates and represent the signal as seen by the radar (i.e., given by time of travel of microwaves). Level 1.5 and 2.0 have been projected into geographic coordinates, such as UTM, or geographic latitude and longitude. The level 1.X data are used for radar interferometry: two images are complex-multiplied to obtain the interferogram. The latter is typically expressed as $A^{-i\phi}$, with amplitude A and phase ϕ. Level 1.5 and 2.0 are expressed as the radar backscatter σ^0. The georeferenced interferogram is seldom distributed and the user is expected to perform the processing. For backscatter, the user has a wide choice of processing level, and can perform radar

processing to specifically enhance or retrieve specific image features. Processing details and analysis to obtain science-ready backscatter images are described in the tutorial.

6.2.6 MAPPING MANGROVE CANOPY STRUCTURE

Forest structure can be described in terms of its spatial extent, spatial heterogeneity, tree cover, canopy height profile, and AGB. However, what can be expected from radar observations of mangrove forest landscapes?

Tree cover, canopy height, and AGB are correlated. However, different radar parameters are used to estimate AGB and forest canopy height. A generic formulation relating radar backscatter to AGB is the following, where a and b are determined by the user from in situ data:

$$\sigma^0(dB) = a + b \times \log(AGB) \ .$$

In wet tropical forests, values are about −22.5 and 3 for a and b, respectively, at L-band. Other equations have also been published, and may require slightly more complex calculation (Yu and Saatchi 2016):

$$\sigma^0(\text{linear}) = Ax^\alpha + (1 - e^{(-Bx)}) + C \ ,$$

where x is the AGB, and A, B, C, and α are coefficients that can be fitted empirically through iteration until x results in the observed σ^0 (linear). For wet tropical forest, the coefficient values are $\alpha = 0.013682$, $A = 0.21116$, $B = 0.051846$, $C = 0.02192$. The coefficient α should be fitted locally. In either case, the fitting parameters can change significantly for mangroves given the variation in structure for a given species and the inundation state. Several authors found radar backscatter decreased significantly with AGB, attributing increased double-bounce scattering at low AGB (e.g., Lucas et al. 2007, Cohen et al. 2013). Nonetheless, one may expect σ^0 to increase with forest AGB up to a saturation value that depends on the radar frequency (i.e., P, L, C, X, K) before it decreases. The longer the wavelength (equivalent to lower frequency), the larger the biomass saturation point (Mougin et al. 1992, Proisy et al. 2002). While general literature is not definite on the backscatter signature of mangrove forests, the upper biomass level detectable with radar is similar to other forests, about 200, 100, 50, and 25 for P, L, C, and X, respectively. After this point, the observed σ^0 reduces due to absorption

by the dense aerial root system found in mangroves (Lucas et al. 2007). This holds for HV; however, observation of scrub mangroves at HH and VV sometimes also display high σ^0 due to increased penetration within the canopy and double-bounce interaction with the water surface or water-saturated ground. While these effects imply estimation of mangrove AGB from backscatter alone is generally difficult and strongly site-dependent, these polarimetric trends (i.e., volume versus double-bounce) can be used to classify mangrove type and also structure (e.g., Hong et al. 2015, Brown et al. 2016), itself related to AGB. For additional information on SAR for biomass estimation, see **Chapter 5**.

It is difficult to map the extent of mangrove forests using radar alone, in particular when the adjacent inland landcover is another forest type. This can also be difficult with optical sensors, as 'color' (e.g., greenness) may not suffice to distinguish mangroves from other vegetation types. Therefore, it is recommended to use a combination of datasets obtained from different sensing technologies (also discussed in **Chapter 3, Sec. 3.5.4**). Landcover classification can generally be performed with the radar backscatter as one of the layers along with data from optical instruments such as Landsat. One can also build upon existing global maps of mangrove extent (e.g., Giri et al. 2011) to extract the area of mangrove forests from the radar data. It is more efficient to start with reliable remote sensing products and improve them rather than reinvent the wheel. Classification can be performed with supervised methods (e.g., maximum likelihood, decision trees, neural network) or unsupervised methods (e.g., ISODATA). Implementations for these algorithms can be found in all major commercial remote sensing software (e.g., ENVI) and also in open source software (QGIS or Python libraries). Training of supervised classifiers requires knowledge of mangrove forest locations that can be easily interpreted by an experienced photo-interpreter or from in situ field surveys. It is important that the training set be representative of the entire range of spectral signature observed with remote sensing. Otherwise, pixels with an untrained spectral signature in radar and optical data, will be thrown into the wrong classes, potentially classified as mangroves. To avoid these issues, an initial unsupervised classification method can be used, followed

by manual merging of 'unsupervised classes' into relevant mangroves classes.

To generate a landcover classification of mangrove forests and type, it is recommended to use radar in combination with different sensing technologies (Nascimento et al. 2013). Discrimination of mangroves against other types of forests inland with L-band data given a priori environmental information (e.g., digital elevation model and water mask) and other sources of optical data such as Landsat (Lucas et al. 2014, Bunting et al. 2018). However, classification results can vary greatly due to availability of polarimetric layers and instrument wavelength and technique. For example, Fonteh et al. (2016) found Sentinel-1 (dual-pol C-band) data did not provide significant improvement over Landsat-based landcover classification, while Zhen et al., found increased accuracy over 10% using fully polarimetric Radarsat-2 data. Aslan et al., 2016, began with a spatial segmentation of an L-band HH and HV dataset, with subsequent Landsat-8 species-specific classification refinement. There exist global maps of mangrove extent derived from optical data (e.g., Giri et al. 2011) that can be used to extract the area of mangrove forests from the radar data. These have recently been improved with L-band radar data from ALOS-1 (Bunting et al. 2018). The authors found it more efficient to start with existing but reliable remote sensing products from Giri et al. (2011) and improve the maps with radar.

There have been significant advances in the use of Radar interferometry to map mangrove canopy height (Simard et al. 2006, Simard et al. 2008, Fatoyinbo et al. 2013, Lagomasino et al. 2015). Data from the SRTM acquired in February 2000, was the first dataset to enable measurement of mangrove canopy height. SRTM was designed to measure elevation, but due to the interaction of the radar microwave with the canopy volume, the SRTM elevation measurement is biased by forest height and density. That is, a forested hill top will appear higher than it is. Assuming mangroves are located at mean sea level with negligible topography, the SRTM elevation measurement is directly related to mangrove canopy height. While this may be a gross assumption in mangrove regions with high tides (>3m), it provides a robust method to determine patterns of mangrove height at

the landscape to global scales in the 2000 epoch. New elevation measurements derived with inter-ferometric data was acquired with TanDEM-X in ~2015, providing a second and more recent dataset (Lee et al. 2015). The TanDEM-X elevation datasets are currently available through a proposal process or can be purchased. An example, calibrated with in situ data, is shown in **Figure 6.8**. Coarser reso-lution data may soon become available.

It is interesting to note that such priori remote sensing products provide a powerful tool to select the location of the in situ plots and optimize cam-paign logistics. Such stratified methods, based on remotely-sensed canopy height, were successfully used in mangrove forests (Trettin et al. 2016, Fatoy-inbo et al. 2018). A similar stratified methodology could also be adopted to train and validate land-cover classification of mangrove structure.

6.3 Conclusions

Radar remote sensing is a powerful tool to mon-itor mangrove extent and map general structure attributes (e.g., trees versus shrubs, aerial root). It enables detection of forest cover changes re-gardless of cloud cover. Used in combination with optical remote sensing observations, radar can improve distinction of mangrove from other types of inland forest. However, the estimation of AGB is limited with radar backscatter alone. Instead, it is recommended to use radar interferometry to accurately map mangrove forest structural attri-butes, including canopy height and aboveground biomass. While fully polarimetric L-band data are freely available (e.g., UAVSAR and ALOS), such datasets at P-, C-, and X- band that span a wide range of mangrove types are rarely accessible. More research on the application of radar remote sensing to study mangrove forests is needed to understand the polarimetric and spectral signa-ture of mangrove forest structure. Nonetheless, recent progress in global mapping and monitoring of mangrove extent (Bunting et al. 2018) and glob-al assessment of AGB (Simard et al. 2019) clearly illustrates the power of radar remote sensing of mangrove forests.
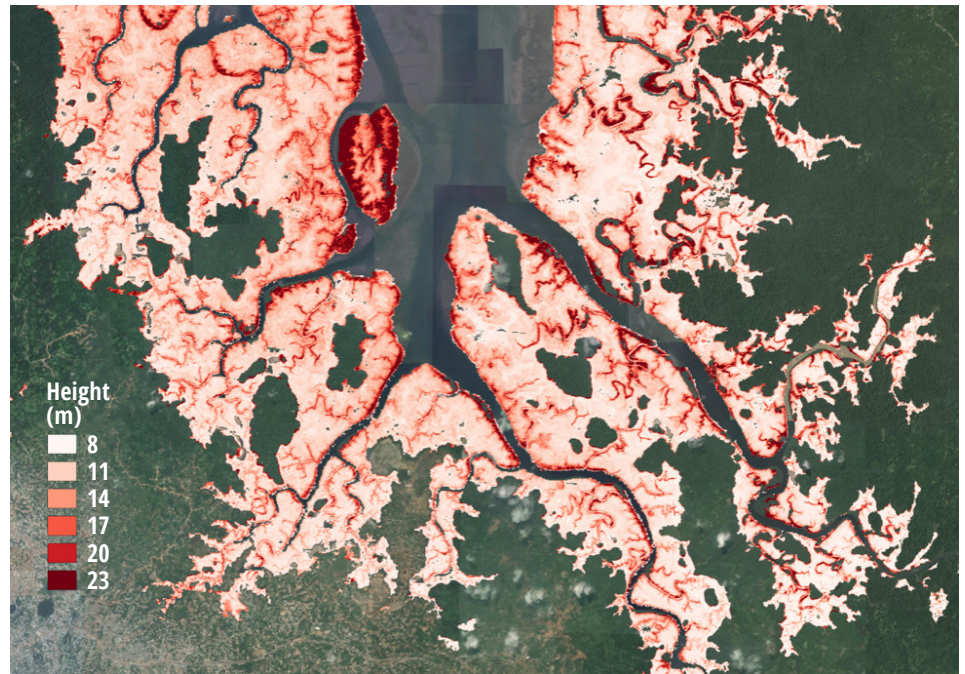

Figure 6.8 *Map of mangrove canopy height in the Akanda National Park obtained from TanDEM-X elevation data (similar to SRTM). Same region as shown **Figure 6.7**.*
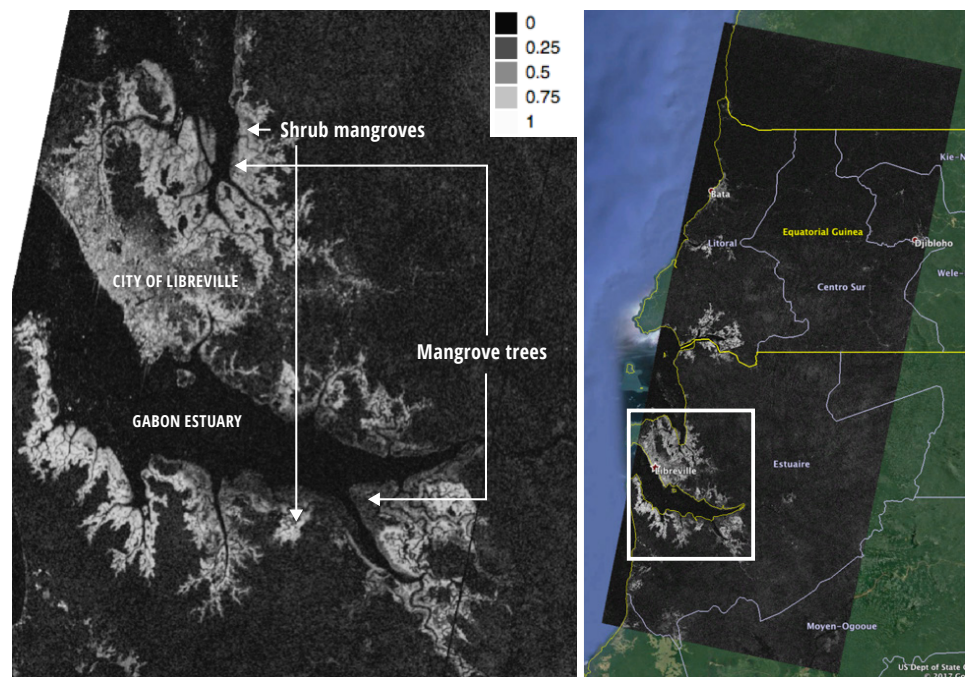

Figure 6.9 *Interferometric radar coherence obtained from ALOS-2 LHH. The bright areas represent coherence close to 1, indicating strong similarity between images collected successively after 24 days. High coherence is observed in open shrub mangroves, as well as in urban areas. Tall mangrove trees exhibit low coherence due to temporal decorrelation caused by scattering in the canopy, which changes between the two radar acquisitions (i.e., 24 days in this case). Open water surface also displays low coherence due to waves constantly changing surface scattering.*

6.4 References

A. Aslan, A. F. Rahman, M. W. Warren, and S. M. Robeson, "Mapping spatial distribution and biomass of coastal wetland vegetation in Indonesian Papua by combining active and passive remotely sensed data," Remote Sens. Environ., vol. 183, pp. 65–81, 2016.

A. Held and C. Ticehurst, "High resolution mapping of tropical mangrove ecosystems using hyperspectral and radar remote sensing," ... Remote Sens., no. October 2014, pp. 37–41, 2003.

Alongi, D. (2002). Present state and future of the world's mangrove forests. Environmental Conservation, 29(3), 331-349. doi:10.1017/S0376892902000231

Arreola-Lizárraga, José Alfredo, Francisco Javier Flores-Verdugo, and Alfredo Ortega-Rubio. "Structure and litterfall of an arid mangrove stand on the Gulf of California, Mexico." Aquatic botany 79.2 (2004): 137-143.

Asbridge, Emma, et al. "Mangrove response to environmental changes predicted under varying climates: case studies from Australia." Current Forestry Reports 1.3 (2015): 178-194.

Barbier, E. B. et al. e value of estuarine and coastal ecosystem services. Ecol. Monogr. 81, 169–193 (2011).

Bunting, P., Rosenqvist, A., Lucas, R., Rebelo, L. M., Hilarides, L., Thomas, N., ... & Finlayson, C. (2018). The Global Mangrove Watch—A New 2010 Global Baseline of Mangrove Extent. Remote Sensing, 10(10), 1669. Data available here : http://data.unep-wcmc.org/datasets/45

Castañeda-Moya, E., Twilley, R. R., & Rivera-Monroy, V. H. (2013). Allocation of biomass and net primary productivity of mangrove forests along environmental gradients in the Florida Coastal Everglades, USA. Forest Ecology and Management, 307, 226-241.

Cheong, So-Min, et al. "Coastal adaptation with ecological engineering." Nature climate change 3.9 (2013): 787.

Cohen, R., J. Kaino, J.A. Okello, J.O. Bosire, J.G. Kairo, M. Huxham, M.Mencuccini. Propagating uncertainty to estimates of above-ground biomass for Kenyan mangroves : A scaling procedure from tree to landscape level. Forest Ecology and Management, vol. 310, pp. 968-982, 2013.

D. C. Donato, J. B. Kauffman, D. Murdiyarso, S. Kurnianto, M. Stidham, and M. Kanninen, "Mangroves among the most carbon-rich forests in the tropics," Nat. Geosci., vol. 4, no. 5, pp. 293–297, 2011.

Denbina, Michael, Marc Simard, and Brian Hawkins. "Forest Height Estimation Using Multibaseline PolInSAR and Sparse Lidar Data Fusion." IEEE Journal of Selected Topics in Applied Earth Observations and Remote Sensing 99 (2018): 1-19.

Duke, Norman, Marilyn Ball, and Joanna Ellison. "Factors influencing biodiversity and distributional gradients in mangroves." Global Ecology & Biogeography Letters 7.1 (1998): 27-47.

E. Mougin, C. Proisy, G. Marty, F. Fromard, H. Puig, J. L. Betoulle, and J. P. Rudant, "Multifrequency and multipolarization radar backscattering from mangrove forests," IEEE Trans. Geosci. Remote Sens., vol. 37, no. 1 PART 1, pp. 94–102, 1999.

Eslami-Andargoli, L., et al. "Mangrove expansion and rainfall patterns in Moreton Bay, southeast Queensland, Australia." Estuarine, Coastal and Shelf Science 85.2 (2009): 292-298.

Fatoyinbo, T. E., et al., (2008). Landscape- scale extent, height, biomass, and carbon estimation of Mozambique's mangrove forests with Landsat ETM+ and Shuttle Radar Topography Mission elevation data. Journal of Geophysical Research 113, G02S06

Fatoyinbo, T.E. & M. Simard (2013). "Height and biomass of mangroves in Africa from ICESat/GLAS and SRTM", International Journal of Remote Sensing, Vol. 34, 2, pp. 668-681.

Fatoyinbo, Temilola E., and Marc Simard. "Height and biomass of mangroves in Africa from ICESat/GLAS and SRTM." International Journal of Remote Sensing 34.2 (2013): 668-681.

Fatoyinbo, Temilola, et al. "Estimating mangrove aboveground biomass from airborne LiDAR data: A case study from the Zambezi River delta." Environmental Research Letters 13.2 (2018): 025012.

Fonteh, M. L., Theophile, F., Cornelius, M. L., Main, R., Ramoelo, A., & Cho, M. A. (2016). Assessing the Utility of Sentinel-1 C Band Synthetic Aperture Radar Imagery for Land Use Land Cover Classification in a Tropical Coastal Systems When Compared with Landsat 8. Journal of Geographic Information System, 8(04), 495.

Freeman, A.; Durden, S.L. A three-component scattering model for polarimetric SAR data. IEEE Trans. Geosci. Remote Sens. 1998, 36, 963–973.

Gilman, Eric L., et al. "Threats to mangroves from climate change and adaptation options: a review." Aquatic botany 89.2 (2008): 237-250.

Giri, C., et al., 2011. Status and distribution of mangrove forests of the world using earth observation satellite data. Global Ecology and Biogeography, 20(1), 154-159

Hansen et al., High-Resolution Global Maps of 21st-Century Forest Cover Change, Science 15 November 2013: 342 (6160), 850-853.

Hashimoto, T.R. Mid-holocene development of mangrove communities featuring rhizophoraceae and geomorphic change in the Richmond River Estuary, New South Wales, Australia. Geographical Research, vol. 44, no. 1, pp. 63 – 76, 2006.

Hutchison, James, et al. "Predicting global patterns in mangrove forest biomass." Conservation Letters 7.3 (2014): 233-240.

I. Brown, S. Mwansasu, and L. O. Westerberg, "L-band polarimetric target decomposition of mangroves of the rufiji delta, Tanzania," Remote Sens., vol. 8, no. 2, 2016.

J. M. Kovacs, X. Jiao, F. Flores-de-Santiago, C. Zhang, and F. Flores-Verdugo, "Assessing relationships between Radarsat-2 C-band and structural parameters of a degraded mangrove forest," Int. J. Remote Sens., vol. 34, no. 20, pp. 7002–7019, 2013.

Jerath, M. An economic analysis of carbon sequestration and storage service by mangrove forests in Everglades National Park, Florida. Master's thesis, Florida International University, 2012.

K. W. Krauss, K. L. McKee, C. E. Lovelock, D. R. Cahoon, N. Saintilan, R. Reef, and L. Chen, "How mangrove forests adjust to rising sea level.," New Phytol., vol. 202, no. 1, pp. 19–34, Apr. 2014.

Kuenzer, C., A. Bluemel, S. Gebhardt, T. V. Quoc, S. Dech. Remote sensing of mangrove ecosystems : A review. Remote Sensing, vol. 3, no.5, pp. 878-928, 2011.

Lagomasino, et al, (2015). High-resolution forest canopy height estimation in an African blue carbon ecosystem. Remote Sensing in Ecology and Conservation, 1(1), 51-60.

Lavalle, Marco, Marc Simard, and Scott Hensley. "A temporal decorrelation model for polarimetric radar interferometers." IEEE Transactions on Geoscience and Remote Sensing 50.7 (2012): 2880-2888.

Lee, SK. et al., "TanDEM-X Pol-InSAR Inversion for Mangrove Canopy Height Estimation," in Selected Topics in Applied Earth Observations and Remote Sensing, IEEE Journal of , vol.8, no.7, pp.3608-3618, July 2015.

Locatelli, Tommaso, et al. "Turning the tide: how blue carbon and payments for ecosystem services (PES) might help save mangrove forests." Ambio 43.8 (2014): 981-995.

Lucas, R. M., Mitchell, A. L., Rosenqvist, A., Proisy, C., Melius, A., & Ticehurst, C. (2007). The potential of L-band SAR for quantifying mangrove characteristics and change: case studies from the tropics. Aquatic Conservation: Marine and Freshwater Ecosystems, 17(3), 245–264. http://doi.org/10.1002/aqc.833

Lucas, R., Rebelo, L. M., Fatoyinbo, L., Rosenqvist, A., Itoh, T., Shimada, M., … Hilarides, L. (2014). Contribution of L-band SAR to systematic global mangrove monitoring. Marine and Freshwater Research, 65(7), 589–603. http://doi.org/10.1071/MF13177

Mayaux, P., P. Holmgren, F. Achard, J. Eva, H. J. Stibig, and A. Branthomme. Tropical forest cover change in the 1990s and options for future monitoring. Philosophical Transactions of the Royal Society B : Biological Sciences, vol. 360, no. 1454, 2005.

M. F. Cougo, P. W. M. Souza-Filho, A. Q. Silva, M. E. B. Fernandes, J. R. Dos Santos, M. R. S. Abreu, W. R. Nascimento, and M. Simard, "Radarsat-2 backscattering for the modeling of biophysical parameters of regenerating mangrove forests," Remote Sens., vol. 7, no. 12, 2015.

M. L. Fonteh, F. Theophile, M. L. Cornelius, R. Main, A. Ramoelo, and M. A. Cho, "Assessing the Utility of Sentinel-1 C Band Synthetic Aperture Radar Imagery for Land Use Land Cover Classification in a Tropical Coastal Systems When Compared with Landsat 8," J. Geogr. Inf. Syst., vol. 08, no. 04, pp. 495–505, 2016.

M. Simard et al., "Mapping Height and Biomass of Mangrove Forests in the Everglades National Park with SRTM Elevation Data", Photogrammetric Engineering & Remote Sensing", Vol. 72, No. 3, March 2006, pp. 299–311.

Mangrove extinction risk and geographic areas of global concern," PLoS One, vol. 5, no. 4, 2010.

McKee, K. L., I. C. Feller, M. Popp, W. Wanek. Mangrove isotopic fractionation across a nitrogen vs. Phosphorus limitation gradient. Ecology : Ecological Society of America, vol. 84, no. 4, pp. 1065-1075, 2002.

McNally, C.G., E. Uchida, and A. J. Gold. The effect of a protected area on the tradeoffs between short-run and long-run benefits from mangrove ecosystems. Proceedings of the National Academy of Sciences of the United States of America, vol. 108, no. 34, pp. 13945 – 13950, 2011.

Mougin, E., A. Lopes, J. Dauzat, D. H. Hoekman, M.A. Karam, A. K. Fung. Interpretation of microwave signatures of trees by a combined backscattering and plant structural model. IGARSS '92 International Geoscience and Remote Sensing Symposium. 26-29 May 1992.

Murray, B. C. Mangroves' hidden value. Nature Climate Change, 2, 773 – 774, 2012.

Nascimento Jr, W. R., et al., 2013. Mapping changes in the largest continuous Amazonian mangrove belt using object-based classification of multisensor satellite imagery. Estuarine, Coastal and Shelf Science, 117, 83-93

O. Hamdan, H. Khali Aziz, and I. Mohd Hasmadi, "L-band ALOS PALSAR for biomass estimation of Matang Mangroves, Malaysia," Remote Sens. Environ., vol. 155, pp. 69–78, 2014.

Pendleton, L., D. C. Donato, B. C. Murray, S. Crooks, W. A. Jenkins, S. Sifleet, C. Craft, J. W. Fourqurean, J. B. Kauffman, N. Marba, P. Megonigal, E. Pidgeon, D. Herr, D. Gordon, A. Baldera.. Estimating global blue carbone from conversion and degradation of vegetated coastal ecosystems. Plos One, vol. 7, 2012.

Pinto, Naiara, Marc Simard, and Ralph Dubayah. "Using InSAR coherence to map stand age in a boreal forest." Remote Sensing 5.1 (2012): 42-56.

Polidoro, B. A., K. E. Carpenter, L. Collins, N. C. Duke, A. M. Ellison, J. C. Ellison, E. J. Farnsworth, E. S. Fernando, K. Kathiresan, N. E. Koedam, S. R. Livingstone, T. Miyagi, G. E. Moore, V. N. Nam, J. E. Ong, J. H. Primavera, S. G. Salmo III, J. C. Sanciangco, S. Sukardjo, Y. Wang, J. W. H. Yong. The loss of species : Mangrove extinction risk and geographic areas of global concern. Plos One, vol. 5, no.4, 1 – 10, 2010.

Primavera, J.H. Development and conservation of Philippine mangroves : Institutional issues. Ecological Economics, vol. 35, no. 1, pp 91 – 106, 2000.

Proisy, C., Mougin, E., Fromard, F., Trichon, V., & Karam, M. A. (2002). On the influence of canopy structure on the radar backscattering of mangrove forests. International Journal of Remote Sensing, 23(20), 4197–4210. http://doi.org/10.1080/01431160110107725

R. M. Lucas, A. L. Mitchell, A. Rosenqvist, C. Proisy, A. Melius, and C. Ticehurst, "The potential of

L-band SAR for quantifying mangrove characteristics and change: case studies from the tropics," Aquat. Conserv. Mar. Freshw. Ecosyst., vol. 17, no. 3, pp. 245–264, May 2007.

Rivera-Monroy, V.H., et al., 2011a. Saiinty and Chlorophyll a as Performance Measures to Rehabilitate a Mangrove-Dominated Deltaic Coastal Region: the Ciénaga Grande de Santa Marta-Pajarales Lagoon Complex, Colombia. Estuaries and Coasts 34: 1-19.

S. E. Hamilton and D. Casey, "Creation of a high spatio-temporal resolution global database of continuous mangrove forest cover for the 21st century (CGMFC-21)," Glob. Ecol. Biogeogr., vol. 25, no. 6, pp. 729–738, 2016.

S. H. Hong, H. O. Kim, S. Wdowinski, and E. Feliciano, "Evaluation of polarimetric SAR decomposition for classifying wetland vegetation types," Remote Sens., vol. 7, no. 7, pp. 8563–8585, 2015.

Saintilan, Neil, et al. "Mangrove expansion and salt marsh decline at mangrove poleward limits." Global change biology 20.1 (2014): 147-157.

Shapiro, A.C., C.C. Trettin, H. Küchly, S. Alvinapanah and S. Bandeira. The mangroves of the Zambezi Delta from 1994-2013: increase in extent observed via satellite. Submitted to Remote Sensing (in review).

Simard, M., L. Fatoyinbo, C. Smetanka, V. H. Rivera-Monroy, E. Castaneda-Moya, N. Thomas, T. Van der Stocken. Mangrove canopy height globally related t o precipitation, temperature, and cyclone frequency. Nature Geoscience, vol. 12, pp. 40-45, 2019.

Simard, M., et al., "A Systematic Method for 3D Mapping of Mangrove Forests Based on Shuttle Radar Topography Mission Elevation Data, ICESat/GLAS Waveforms and Field Data: Application to Ciénaga Grande de Santa Marta, Colombia," Remote Sensing of the Environment, Vol. 112/5, pp. 2131-2144, 2007.

Simard, M., Fatoyinbo, T., Smetanka, C., Rivera-Monroy, V., Castaneda-Moya, E., Thomas, N., & Van der Stocken, T. (2019). Mangrove canopy height globally related to precipitation, temperature and cyclone frequency. Nature Geoscience, 12(January). http://doi.org/10.1038/s41561-018-0279-1

Simard, Marc, et al. "A systematic method for 3D mapping of mangrove forests based on Shuttle Radar Topography Mission elevation data, ICEsat/GLAS waveforms and field data: Application to Ciénaga Grande de Santa Marta, Colombia." Remote Sensing of Environment 112.5 (2008): 2131-2144.

Simard, Marc, et al. "An empirical assessment of temporal decorrelation using the uninhabited aerial vehicle synthetic aperture radar over forested landscapes." Remote Sensing 4.4 (2012): 975-986.

Simard, Marc, et al. "Mapping height and biomass of mangrove forests in Everglades National Park with SRTM elevation data." Photogrammetric Engineering & Remote Sensing 72.3 (2006): 299-311.

Soares, Mário Luiz Gomes, et al. "Southern limit of the Western South Atlantic mangroves: As-

sessment of the potential effects of global warming from a biogeographical perspective." Estuarine, Coastal and Shelf Science 101 (2012): 44-53.

Souza-Filho, P. W. M., et al. 2011. Discrimination of coastal wetland environments in the Amazon region based on multi-polarized L-band airborne Synthetic Aperture Radar imagery. Estuarine, Coastal and Shelf Science, 95(1), 88-98.

Spalding, M., F. Blasco, C. Field. World Mangrove Atlas. International Society for Mangrove Ecosystems, WCMC, National Council for Scientific Research, Paris, 1997.

Spalding, M., et al., 2010. World atlas of mangroves. Earthscan.

T. C. Jennerjahn and V. Ittekkot, "Relevance of mangroves for the production and deposition of organic matter along tropical continental margins," Naturwissenschaften, vol. 89, no. 1, pp. 23–30, 2002.

Thomas, N., Lucas, R., Bunting, P., Hardy, A., Rosenqvist, A., & Simard, M. (2017). Distribution and drivers of global mangrove forest change, 1996–2010. PloS one, 12(6), e0179302.

Trettin, Carl C., Christina E. Stringer, and Stanley J. Zarnoch. "Composition, biomass and structure of mangroves within the Zambezi River Delta." Wetlands ecology and management 24.2 (2016): 173-186.

Valiela, I., J. L. Bowen, J. K. York. Mangrove Forests : One of the world's threatened major tropical environments : at least 35% fo the area of mangrove forests has been lost in the past two decades, losses that exceed those for tropical rain forests and coral reefs, two other well-known threatened environments. BioScience, vol. 51, no. 10, pp 807 – 815, 2001.

Vo, Quoc Tuan, et al. "Review of valuation methods for mangrove ecosystem services." Ecological indicators 23 (2012): 431-446.

Wilson, Nicholas C., and Neil Saintilan. "Growth of the mangrove species Rhizophora stylosa Griff at its southern latitudinal limit in eastern Australia." Aquatic botany 101 (2012): 8-17.

Yu, Y. and S. Saatchi. (2016). Sensitivity of L-band SAR Backscatter to aboveground biomass of global forests. Remote Sensing, 8(6), 522.

Zhen, J., Liao, J. and Shen, G., 2018. Mapping Mangrove Forests of Dongzhaigang Nature Reserve in China Using Landsat 8 and Radarsat-2 Polarimetric SAR Data. Sensors, 18(11), p.4012.

DR. MARC SIMARD is a Senior Scientist with NASA-Jet Propulsion Laboratory's Radar Science & Engineering Section. He obtained a PhD in Geomatics in 1998 at the Université Laval, Québec. Simard is also a Project Scientist within the Joint Institute for Regional Earth System Science at the University of California in Los Angeles (UCLA). He is also an Adjunct Faculty member at the Department of Oceanography and Coastal Sciences of Louisiana State University (LSU). He is an active member of the International Blue Carbon Working Group (the Blue Carbon Initiative is sponsored by Conservation International, UNEP and IUCN) and JAXA's Global Mangrove Watch program.

Since 2004, Dr. Simard has served as the Principal or Co- Investigator of several NASA funded projects in the Carbon Cycle and Ecosystems (CC&E) program. His research has a strong multi-disciplinary dimension with a focus on coastal wetlands regions. He is currently, among other NASA projects, a co-investigator in a NASA Carbon Monitoring System (CMS) for mangrove forests entitled: "Estimating Total Ecosystem Carbon in Blue Carbon and Tropical Peatland Eco-systems".

Marc Simard was the Principal Investigator for the JPL funded 2016 multi-aircraft campaign in the Mississippi River Delta, a precursor to Delta-X. Finally, and highly relevant, Simard is a member of the Science Teams of two upcoming NASA spaceborne missions: NISAR (NASA-ISRO Synthetic Aperture Radar) and SWOT (Surface Water and Ocean Topography) both planned for launch in 2021. Dr. Simard expects that, in addition to providing deep understanding of ac-cretion processes, the Delta-X data will be used for the NISAR and SWOT cal/val, and enhance these NASA missions.

Simard, Marc. "Radar Remote Sensing of Mangrove Forests." SAR Handbook: Comprehensive Methodologies for Forest Monitoring and Biomass Estimation. Eds. Flores, A., Herndon, K., Thapa, R., Cherrington, E. NASA 2019. DOI: 10.25966/33zm-x271